

The influence of collective neutrino oscillations on a supernova r process

Huaiyu Duan

Department of Physics and Astronomy, University of New Mexico, Albuquerque, NM 87131, USA

Alexander Friedland

Theoretical Division, Los Alamos National Laboratory, Los Alamos, NM 87544, USA

Gail C. McLaughlin

Department of Physics, NC State University, Raleigh, NC 27695-8202, USA

Rebecca Surman

Department of Physics and Astronomy, Union College, Schenectady, NY 12308, USA

ABSTRACT: Recently, it has been demonstrated that neutrinos in a supernova oscillate *collectively*. This process occurs much deeper than the conventional matter-induced MSW effect and hence may have an impact on nucleosynthesis. In this paper we explore the effects of collective neutrino oscillations on the r -process, using representative late-time neutrino spectra and outflow models. We find that accurate modeling of the collective oscillations is essential for this analysis. As an illustration, the often-used “single-angle” approximation makes grossly inaccurate predictions for the yields in our setup. With the proper multiangle treatment, the effect of the oscillations is found to be less dramatic, but still significant. Since the oscillation patterns are sensitive to the details of the emitted fluxes and the sign of the neutrino mass hierarchy, so are the r -process yields. The magnitude of the effect also depends sensitively on the astrophysical conditions — in particular on the interplay between the time when nuclei begin to exist in significant numbers and the time when the collective oscillation begins. A more definitive understanding of the astrophysical conditions, and accurate modeling of the collective oscillations for those conditions, is necessary.

KEYWORDS: neutrinos, supernovae, nucleosynthesis.

1. Introduction

There are a number of types of element synthesis that are thought to occur in “hot outflows”, such as the formation of light p -process elements, possibly r -process elements, and also some iron peak elements. A hot outflow is one in which nucleons are originally photo-dissociated into free nucleons at temperatures of around a few tens of MeV. Material typically flows away from a hot center, such as an accretion disk around a black hole or proto-neutron star, and as it does so the nucleons cool and combine into nuclei. Given the high temperature of the center, neutrinos can be emitted in vast numbers. These neutrinos interact with the outflowing and cooling nucleons and nuclei and, among other things, change neutrons into protons and vice-versa. Thus any process which alters the luminosity or spectra of the neutrinos may impact element synthesis. Neutrino flavor transformations – and, specifically, collective oscillations, as explained later – are a prime example of such a process and it is essential to determine whether they are important for nucleosynthesis in hot outflow environments. In this initial work we explore, by considering a few specific examples, the size of this effect on the abundances of rapid neutron capture elements.

It should be stressed that the physics underlying the oscillations is by now well established and treating it is no longer optional. The essential ingredients are the measured neutrino oscillation parameters and, crucially, the neutrino-neutrino coherent interactions [1, 2, 3, 4, 5, 6], which can cause *collective* oscillations. It has been suspected for nearly two decades that neutrino oscillations (*e.g.*, [7]), particularly the collective oscillations between the active flavors [8, 9, 10, 11, 12], could potentially impact the r -process. The case for this became much stronger in the last five years, since supercomputer calculations of collective oscillations have become available (starting with [13, 14]). These calculations have shown that, even without sterile neutrinos, large flavor transformations can develop sufficiently close to the neutrinosphere, where the r -process is thought to occur. Yet, with the exception of the recent attempt [15], the impact of the new results on the r -process has not been investigated.

The reason for this, we believe, is not the lack of interest, but the inherent complexity of the problem. First, accurate modeling of collective oscillations requires supercomputers. This is so because – unlike the more familiar MSW flavor transformations, in which each neutrino evolves independently – in the collective oscillation regime neutrinos of different directions and different energies are coupled [9, 13]. Second, one has a chain of nuclear reactions to follow, as a function of the position in the outflow. Lastly, the physical conditions, in which the candidate r -process takes place, themselves require detailed simulations.

In its full form, this is clearly a very ambitious program. The goal of the present paper is to gauge the effect and establish whether or not its magnitude warrants further, more detailed modeling. Moreover, we would like to get a sense of the size of the effect for a variety of conditions. With these goals in mind, we pick astrophysical conditions which produce neutron rich outflow, following models in the existing literature. Since collective effects may cause rapid oscillations above the neutrinosphere, we couple neutrino transformation calculations to a nuclear reaction network. We present several examples of calculations obtained in this

way. One may attempt to reduce the impact of the oscillations on the r -process to a simple criterion, such as the electron fraction Y_e at a certain radius. Such prescriptions should also be applied with care and we discuss their limitations.

One is also tempted to simplify the treatment of the collective oscillations. We show, however, that such simplifications may lead to entirely erroneous results. We illustrate this with the example of the frequently used “single-angle” approximation, which in this case is seen to utterly fail. This sensitivity to the details of the oscillations – and, correspondingly, the need to model this process carefully – is one of the major results of this paper.

Lastly, although our outflow models are clearly simplified (and, indeed, as explained in the next Section, the exact mechanism of the astrophysical r -process is yet to be conclusively established), we believe our basic framework and findings should apply more generally. For example, NS-NS and BH-NS mergers also have neutrinos which, for hot outflows, strongly influence the composition of the accretion disk and outflow [16, 17]. We will return to this important point at the end.

This paper is organized as follows. In Sect. 2, we briefly summarize the current status of the r -process modeling. In Sect. 3, we illustrate the effects of neutrino flavor transformations using a toy model. In Sect. 4, we introduce the main physics of the collective transformations and give order-of-magnitude arguments why these transformations may impact the r -process. In Sect. 5, we describe the nucleosynthesis network calculations and, in Sect. 6 we present our sample results. Finally, in Sect. 7, we summarize our findings and discuss them in a more general context of astrophysical nucleosynthesis.

2. Overview of the r -process

The abundance pattern of elements [18, 19] in the region between the $A = 130$ peak and the actinides is consistent with the rapid neutron capture process (r -process [20, 21]; see [22] for a recent review). There is a long-standing question regarding the origin of the r -process. Astrophysical data points to a phenomenon that happens early in the evolution of the universe and has a relatively high frequency [23, 24, 25, 26]. Neutron star - neutron star (NS-NS) mergers [27, 28] and black hole-neutron star (BH-NS) mergers [29, 16] are difficult to reconcile with this data [30, 31]. On the other hand, core collapse supernovae (CCSN) do have the right timescale. This motivates a closer look at possible r -process conditions in these objects.

Unfortunately, the exact mechanism by which CCSN produce an r -process has not yet been conclusively established. The neutrino driven wind is a popular environment to study [32, 33], but there is by now a long series of papers in the literature that show that it is more difficult to produce the requisite conditions than first thought, e.g. [34, 35, 36, 37, 38, 39, 40, 41, 42].

Solutions to this problem may come from a better understanding of the relevant physics. To this end, as a necessary step, one should identify and quantify all physical processes that may impact the r -process yields (whether or not they solve the problem). Suggestions have

been made, for instance, regarding neutrino physics [43, 44, 45, 46, 47] and hydrodynamics [48, 49]. As another example, fission cycling could produce a good fit to the data [50, 51] but the electron neutrino fraction would have to be much lower than is predicted by any model, e.g. [45, 46] for a recent example, save those that include sterile neutrinos [52, 53, 54, 55].

Our present investigation of the effects of neutrino oscillations may be viewed as part of this larger effort to identify and quantify all relevant physics that could significantly impact the r -process yields. At the same time, we wish to set up a framework, which should apply for a variety of conditions. Whatever the final solution to the r -process is, one may need to address if and how the neutrino oscillations impact the yields.

3. Toy model

We begin our study of the influence of collective oscillations on the r -process by examining a toy model of the supernova neutrino-driven wind. In the traditional picture of this environment, material initially composed of free nucleons is heated to high entropy by the neutrinos emitted from the cooling protoneutron star. The heated material expands outwards and cools adiabatically; as the temperature drops the nucleons assemble first into alpha particles and then into heavier nuclei. Studies have shown that r -process nucleosynthesis can proceed in this environment if (a) there is a neutron excess in the initial composition (i.e., the initial electron fraction $Y_e = 1/(1 + n/p)$ is less than 0.5), (b) the entropy is sufficiently high to favor lighter nuclei at high temperatures, and (c) the timescale is sufficiently fast to lower the efficiency of converting alpha particles to heavier nuclei. If the first condition is satisfied, the latter two conditions are necessary to achieve the large neutron-to-seed ratio required for a robust r -process. Note that this first condition (a) is only a guideline and not a strict requirement, since it has been shown that in certain cases r -process elements can be produced under proton rich conditions [56].

Neutrinos play an important role in each stage of the nucleosynthesis. Weak interactions on nucleons



are responsible for setting the electron fraction Y_e in the ejected material. In regions most relevant for nucleosynthesis, electron neutrino captures on neutrons and electron antineutrino captures on protons dominate. If the electron antineutrino spectrum is hotter than the electron neutrino spectrum, as is traditionally assumed for the late-time neutrino emission from a cooling protoneutron star, then the rate of electron antineutrino captures will be faster and a composition with more neutrons than protons will be favored. The neutrino physics is therefore responsible for the initial neutron excess crucial for the r -process.

When the temperature in the outflow drops to the point where nuclear reassembly begins, all of the protons (and a corresponding number of neutrons) become locked up in alphas,

shutting off the electron antineutrino captures on protons that produce free neutrons. At this point, electron neutrino interactions on neutrons act to reduce the available free neutron abundance directly and also indirectly, as the protons produced by the neutrino captures bind with additional free neutrons to form alpha particles. This is the so-called ‘alpha effect’ detailed in [35, 36, 37]. After the epoch of alpha particle formation is past, electron neutrino interactions continue to reduce the availability of free neutrons but the effect weakens as the material moves away from the protoneutron star.

If the traditional hierarchy of neutrino energies is assumed, i.e. $\langle E_{\nu_{\mu,\tau}} \rangle > \langle E_{\bar{\nu}_e} \rangle > \langle E_{\nu_e} \rangle$, then e, μ, τ flavor oscillations *may* act to raise the effective energies of the ν_e and $\bar{\nu}_e$ fluxes. This has important nucleosynthetic consequences, with the severity determined by which the stage the nucleosynthesis is in when the flavor transformation occurs. If the transformation happens at early times, when the composition of the material is mostly free nucleons, the electron fraction will readjust. A transformation that takes place when the composition is dominated by alphas will enhance the alpha effect, and a transformation that occurs after seeds form will reduce the number of free neutrons available for capture during the r -process.

Of course, the impact of the oscillations should depend on the details of the process, particularly on which parts of the spectra are permuted and at which distances. This requires detailed modeling of the oscillations, which is presented later. Here, we would like to illustrate these effects, assuming the oscillations lead to a simple swap of entire spectra between flavors.

We present the results from such a toy calculation in Fig. 1. We took the neutrino fluxes to be the late-time fluxes from [57], specifically the simulation labeled $q = 3.0$. It describes spectra of the form $\propto E^2[1 + \exp(E/T - \eta)]^{-1}$, with neutrino temperatures $T_{\nu_e} = 2.6$, $T_{\bar{\nu}_e} = 4.0$ MeV, and $T_{\nu_\mu} = 5.0$ MeV, degeneracy parameters $\eta_{\nu_e} = 3.0$, $\eta_{\bar{\nu}_e} = 2.8$, and $\eta_{\nu_\mu} = 1.8$, and luminosities $L_{\nu_e} = 6.6 \times 10^{51}$ ergs s $^{-1}$, $L_{\bar{\nu}_e} = 8.8 \times 10^{51}$ ergs s $^{-1}$, and $L_{\nu_\mu} = 12.7 \times 10^{51}$ ergs s $^{-1}$. These neutrino parameters set the initial electron fraction of the material at $Y_e = 0.41$. (Note that recent calculations of proto-neutron star evolution predict neutrino parameters that produce higher electron fractions and would require more extreme conditions to produce r -process elements than those used here [45, 46].) We chose a sample hydrodynamic trajectory that results in a main r -process for the given neutrino parameters. We then ran four simulations, one with neutrino interactions turned off after the electron fraction was set, one with unchanged neutrino fluxes throughout, and the remaining two with toy neutrino swaps, where the electron neutrino flux was simply replaced by the μ neutrino flux at a specified radius. A comparison between the simulations with unchanged neutrino physics and with no neutrino interactions for $T < 10^{10}$ K show the operation of the normal alpha effect, whereby neutrino interactions on neutrons result in more alphas and fewer neutrons (top panel of Fig. 1) and a less robust $A \sim 195$ peak in the final r -process abundance distribution (bottom panel of Fig. 1). A neutrino flavor swap that takes place after alpha particle formation acts to enhance the alpha effect; the toy swap increases the alpha particle mass fraction, decreases the neutron abundance, and weakens the resulting r -process. A neutrino flavor swap that takes place while the composition is dominated by free nucleons causes a readjustment of the neutron-to-proton ratio and an even stronger alpha effect, with

a dramatic influence on the subsequent r -process, which in this case does not go beyond the $A \sim 130$ peak.

Our toy model confirms that the influence of the neutrino flavor transformations on supernova nucleosynthesis depends sensitively on what stage of nucleosynthesis the material is in when the transformation occurs. This is determined by the hydrodynamic trajectory of the outflowing material. Fig. 2 shows approximate temperature ranges for each stage of the nucleosynthesis along with the temperature as a function of radius for two sample hydrodynamic trajectories, described in Section 5. Fig. 2 also shows a sample electron neutrino survival probability $P(e)$ for 20 MeV neutrinos, calculated as described in Section 4 below. In this example, the maximum rate of the flavor transformation occurs at roughly 140 km from the neutron star. For the lower entropy trajectory shown by the dashed line, this corresponds to the assembly of seed nuclei, and so we anticipate the nucleosynthetic consequences to be similar to that shown by the purple line in the toy model plot, Fig. 1. For the higher entropy trajectory given by the dot-dashed line in Fig. 2, the same location corresponds to an earlier stage of nucleosynthesis, namely, the assembly of alpha particles. The influence of the flavor transformation is expected to be more dramatic here, closer to that shown by the red line of Fig. 1. Since large uncertainties remain in the astrophysical conditions of the r -process, we investigate the nucleosynthesis using a sampling of parameterized wind trajectories in which the swap may occur during earlier or later stages in the nucleosynthesis.

4. Collective neutrino oscillations

Let us now turn to modeling neutrino flavor oscillations. As we mentioned earlier, the main mechanism of flavor conversion that is relevant to r -process nucleosynthesis is the collective oscillations, caused by coherent neutrino-neutrino interactions, rather than the more familiar MSW (matter-enhanced) conversion. We begin by reviewing the two processes.

Outside of the neutrinosphere, the neutrinos by definition do not experience any incoherent scattering. Yet, their *coherent forward* scattering on the background particles remains important for the flavor evolution. The MSW effect [58, 59] is the textbook example of this phenomenon. The scattering involved in this process is on electrons, protons, and neutrons of the medium. The MSW process is well known to operate in the Sun and should also operate in the supernova environment, as was recognized early on [60]. Yet, for the conditions typical of an iron core supernova, this process does not impact the r -process.

To see this, consider the condition for the transformation, which is given by the comparison of the vacuum and matter terms in the neutrino oscillation Hamiltonian,

$$\Delta m^2/2E_\nu \sim \sqrt{2}G_F N_e. \quad (4.1)$$

The l.h.s. is either of the two eigenvalue splittings in the vacuum oscillation term; the r.h.s. is the corresponding splitting in the Wolfenstein matter term. Here, E_ν is the neutrino energy, N_e is the number density of background electrons and Δm^2 is either $\sim 7.7 \times 10^{-5}$ eV², or

$\sim 2.7 \times 10^{-3} \text{ eV}^2$, corresponding to the “solar” and “atmospheric” mass splittings. Both Δm^2 values lead to flavor transformations, although the details of the transformations differ ¹.

The important point is that in an iron core collapse supernova, either “atmospheric” or “solar” MSW transformations typically occur at large radii, beyond those of interest for the r -process. Indeed, it follows from Eq. (4.1) that for typical neutrino energies of $\sim 10 \text{ MeV}$ and the electron fraction of $Y_e \sim 0.4$, the “atmospheric” transformation takes place at densities of $\sim 10^3 \text{ g/cm}^{-3}$ and the “solar” one at still lower densities. Comparing this with the wind profiles in Fig. 3, we see that the MSW transformations occur at $r \gtrsim 500 \text{ km}$, by which point even the formation of the seeds is complete (Fig. 2).

Let us now turn to collective oscillations. Let us note at the outset that the physics of this phenomenon has been shown to be very rich. The subject is still being actively explored and even a complete discussion of the established results would be well beyond the scope of the present paper. The reader is encouraged to consult specialized literature on the subject (*e.g.*, [62, 63] and references therein). Our goal here is to introduce the basic relevant physics and explain, using simple order-of-magnitude considerations, why this effect could be relevant to the r -process.

The starting observation is that during the first $\mathcal{O}(10)$ seconds of the explosion the number density of streaming neutrinos N_ν in a supernova is very high. Because of this, close to the neutrinosphere, their mutual coherent scattering is physically important [1, 2, 3, 4, 5, 6]. In addition to the vacuum oscillation term and the Wolfenstein matter term, the oscillation Hamiltonian in this regime contains the term induced by the neutrino background [3, 4],

$$H_{\nu\nu}^{(j)} = \sum_i \sqrt{2} G_F N_\nu (1 - \cos \Theta_{ij}) |\psi_i\rangle \langle \psi_i| - \sum_{\bar{i}} \sqrt{2} G_F N_{\bar{\nu}} (1 - \cos \Theta_{\bar{i}j}) |\psi_{\bar{i}}^*\rangle \langle \psi_{\bar{i}}^*|. \quad (4.2)$$

The index i runs over all neutrino groups and \bar{i} over all antineutrino groups. The index j refers to the neutrino group for which the equation is written: different groups are characterized by different energies and/or directions. The interaction strength between any two groups depends of the angle between particle momenta, Θ_{ij} ($\Theta_{\bar{i}j}$).

The evolution Hamiltonian for each neutrino group now contains contributions from all neutrinos in the ensemble. Therefore, flavor evolutions of neutrinos and antineutrinos, of different flavors, energies and on different trajectories become coupled. Thus, despite being superficially similar to the Wolfenstein matter term, the neutrino-neutrino term, where it is important, brings about qualitative change to the problem. The neutrino ensemble now evolves *collectively*.

What is the condition for the neutrino-neutrino term to be physically important? By analogy with Eq. (4.1), one may start by comparing the dimensionful coefficient in Eq. (4.2)

¹In the limit of the small mixing angle, the MSW transformation occurs either in neutrinos or in antineutrinos (depending on where the resonance is, which, in turn, depends on the sign of the mass hierarchy). This regime applies to the “atmospheric” transformation, since it is controlled by the small θ_{13} angle. In contrast, the “solar” mixing angle is large and *both* neutrinos and antineutrinos transform, at similar densities. The notion of “resonant” vs. “nonresonant” transformation is not physically useful here. To this end, note that Eq. (4.1) does not contain the factor of $\cos 2\theta$ that is present in the traditional definition of the resonance [61].

to those of the neutrino-matter interactions and the vacuum oscillation term. This gives (*e.g.*, [64]), $|N_\nu - N_{\bar{\nu}}| \gtrsim |N_{e^-} - N_{e^+}|$ and $G_F |N_\nu - N_{\bar{\nu}}| \gtrsim \Delta m^2 / E_\nu$, correspondingly.

The next step is to account for the angular factors in Eq. (4.1), which are important for the conditions specific to the supernova. Indeed, at sufficiently large distances from the neutrinosphere neutrino rays becomes nearly collinear and therefore the geometric factors $(1 - \cos \Theta)$ become parametrically small. Comparing the neutrino self-interaction term to the vacuum oscillation term, one gets

$$G_F |N_\nu - N_{\bar{\nu}}| \langle 1 - \cos \Theta(r_{\nu\nu}) \rangle \gtrsim \Delta m^2 / E_\nu. \quad (4.3)$$

Here, the brackets denote an appropriate averaging over angles. The l.h.s. falls rapidly with radius, as $\propto N_\nu(r)(1 - \cos \Theta) \propto r^{-4}$ [8], suggesting that any transformations have to occur close to the neutrinosphere. Indeed, given the late-time emission rate of $\sim 10^{51}$ erg/s/10 MeV $\sim 10^{56}$ neutrinos per second, the radius of the neutrinosphere $R_\nu \simeq 10$ km, and the atmospheric $\Delta m^2 = 2.7 \times 10^{-3}$ eV², Eq. (4.3) gives $r_{\nu\nu} \sim \mathcal{O}(100 \text{ km})$.

Importantly, a similar geometric correction does not apply when comparing the neutrino self-interaction term to the background matter term (which would suppress collective oscillations). This is because the overall effect of the background matter can be “rotated away”, as explained in [65]. This important physical result is the reason why large collective flavor transformations do occur under realistic supernova conditions [13, 14]. The residual dispersion of the matter phase on different trajectories, however, cannot be rotated away, so that very dense matter does suppress collective oscillations [66]. The comparison of this dispersion to neutrino self-interaction strength shows the inequality

$$|N_\nu - N_{\bar{\nu}}| \gtrsim |N_{e^-} - N_{e^+}| \quad (4.4)$$

is unmodified [66].

Note that the same argument applies to the vacuum oscillation term, but in this case the dispersion with energy is of the same size as $\Delta m^2 / E_\nu$. Still, strictly speaking, it should be understood that the r.h.s. of Eq. (4.3) contains *the dispersion* of the vacuum term (with antineutrinos counting as negative energies).

Lastly, one should also consider the dispersion of the neutrino self-interaction on different trajectories. It can be easily shown that, similarly to the matter term, this dispersion is comparable to the average strength of the interaction [67]. In the frequently used *single-angle* approximation, this dispersion is neglected by fiat (and the calculation considerably simplifies as a result). The justification for this approximation came not from any first principles argument, but rather from comparing the results of single-angle and multiangle calculations in certain setups. On the other hand, as shown in [67], single-angle calculations do not always reproduce full multiangle results. In cases when they disagree, the dispersion in neutrino self-interaction term can lead to the suppression of the oscillations close to the neutrinosphere. The condition for the oscillations is

$$|N_\nu - N_{\bar{\nu}}| \langle 1 - \cos \Theta(r_{\nu\nu}) \rangle \sim \Delta m^2 / (G_F E_\nu), \quad (4.5)$$

e.g., the inequality in Eq. (4.3) becomes an approximate equality; flavor transformations occur just before the neutrino-neutrino interaction ceases being physically important (*cf* Eq. (4.3)). This multiangle suppression proves crucial for the analysis of the r -process, as we show in what follows.

To recapitulate, Eqs. (4.3) and (4.4) give the *necessary* conditions for the neutrino flavor transformations, if any, to be in the collective regime. These equations, however, do not tell what that evolution is: this is the question of dynamics. With this in mind, we finally turn to our modeling of the oscillations.

Since we are interested in the r -process in the neutrino driven wind environment, we specialize to the late-time spectra, taken from [57]. As our baseline scenario, we choose the $q = 3.0$ point from Table 6 in that paper, as described in the previous Section. The matter density profiles we use are shown in Fig. 3. The densities are low enough so that the matter suppression mechanism does not delay the onset of the oscillations. On the other hand, the anisotropy-driven (multiangle) suppression is present for these spectra. While in the single-angle calculations the oscillations start right away, as the neutrinos are released, in the multiangle treatment the oscillations are delayed.

This is qualitatively similar to what is described in [67], although it must be stressed that the quantitative details are different, in ways that are important for the r -process. Unlike in [67], where the multiangle calculations predicted oscillations starting at ~ 125 km, here we find the oscillations start at ~ 75 km. This difference is due to the choice of the initial spectra: here, as mentioned above, we use the $q = 3.0$ spectra from Table 6 in [57], while the computations in [67] are done for the $q = 3.5$ spectra. We consider the $q = 3.0$ spectra here because they create conditions more suitable for the r -process.

We consider oscillations between all three known neutrino flavors, since three-flavor evolution may be entirely different from the two-flavor approximation (*e.g.*, [68]). We use the known solar and atmospheric neutrino oscillation parameters, set the value of the unknown angle θ_{13} to 0.01, and consider both signs of the neutrino mass hierarchy. The starting radii for the oscillations with our baseline spectra happen to be the same for the normal and inverted mass hierarchies. The oscillation patterns, however, develop differently in the two cases and therefore the impact on the nucleosynthesis needs to be considered separately. The dependence on the hierarchy becomes even more obvious as one varies the spectra. As an illustration, we vary the luminosities of the non-electron neutrino flavors, L_x . With L_x suppressed by a factor of 0.7, for example, the starting radius for oscillations becomes 70 km for the inverted hierarchy, while for normal hierarchy the collective oscillations disappear altogether. This sensitivity of the starting radius on the details of the assumed spectra is, in fact, an important generic feature of the collective oscillations in this regime. We will show how these changes impact the r -process predictions.

Lastly, a word of caution: one should exercise care when applying oscillation results available in the literature to the r -process calculation. Most papers on collective oscillations are typically focused on modeling the neutrino signal in a terrestrial detector. Correspondingly, the neutrino spectra are typically reported at sufficiently large radii, chosen so that the trans-

formations have completed. Typically, at this stage one finds a pattern of spectral “swaps”, *i.e.*, neutrinos of different flavors exchange spectra in certain energy intervals. It would be completely incorrect to use these final spectra to model the r -process. Indeed, the swaps are formed only at hundreds of kilometers from the collapsed core. What we need instead is the detailed information of how the oscillations develop early on, not what they finally settle to. That is why we compute our oscillations “from scratch”.

5. Nucleosynthesis calculation

For the full nucleosynthesis calculations, we begin with a nuclear statistical equilibrium calculation [52] to follow the composition of free nucleons and alphas at high temperature, switch to an intermediate mass nuclear network calculation [69] to determine the mass fractions of the seed nuclei, and finally finish with a simplified nuclear network calculation (including neutron capture, photodissociation, beta decay, beta-delayed neutron emission, and charged-current neutrino interactions) [70] to find the final r -process abundances.

For our studies we use a modified neutrino driven wind model. Neutrino driven wind models were first developed by [71] and were then improved upon by [72, 74, 73, 75]. Recently, it has been shown that the traditional exponential outflow should be modified by a slowdown as the neutrino heated material reaches the supernova shockfront [48].

Here we use a range of adiabatic wind trajectories based on the parameterization of Panov and Janka [76]. The parameterization in [76] takes the first stage of the outflow to be a steady-state expansion with an exponentially-growing radius, $r(t) = r_{\text{init}}e^{t/\tau}$, and an exponential decline in density, $\rho = \rho_{\text{init}}e^{-t/3\tau}$, where τ is the initial dynamical timescale. In the second stage of the outflow, corresponding to its evolution after deceleration by a reverse shock, the density declines more slowly, as a power law $\rho = \rho_0(t/t_0)^{-2}$, where ρ_0 and t_0 are the density and time at the point of transition to the power law dependence, taken in [76] to be the time at which the temperature is $T_9 = 1$. The steady-state condition $r^2\rho v = \text{constant}$ is used to find $r(t)$ and $v(t)$.

We use this parameterization to calculate two density profiles $\rho(r)$, shown in Fig. 3, that are roughly consistent with, but not fit to, early-type and late-type density profiles from Arcones *et al* [48]. We then generate a range of hydrodynamic and thermodynamic trajectories from these profiles by varying entropy and initial timescale. The constant entropy is used to calculate temperature from the density, and the initial timescale determines the evolution of the velocity, which is calculated from the steady-state condition $r^2\rho v = \text{constant}$. Note that this parameterization differs from that of [76] only in how the switchover point from exponential to power law is determined; here it is not set by a temperature condition but from the density profile. We examine trajectories with a variety of entropies, $s/k = 100, 200, 300$, and a range of initial timescales, $1 \text{ ms} < \tau < 50 \text{ ms}$.

The neutrino fluxes and survival probabilities calculated as described above were output every kilometer from 40 to 1000 km for the nucleosynthesis calculation. The electron neutrino and antineutrino capture rates per nucleon that result are shown in Fig. 4 as a function of

radius, compared to the rate assuming no oscillations. While the neutrino capture rates are unchanged close to the neutron star, collective oscillations increase the rates farther out, by up to factors of two to three.

We note that previous work [12, 15] on the influence of collective oscillations on nucleosynthesis have relied upon calculations of the equilibrium electron fraction to provide a first estimate of the type of nucleosynthesis likely in the outflow. This equilibrium electron fraction is approximated as $Y_e = 1 / \left(1 + \frac{\lambda_{\bar{\nu}_e}}{\lambda_{\nu_e}} \right)$. This equation comes from the more general [36]

$$\begin{aligned} \dot{Y}_e = & (\lambda_{\nu_e, n} + \lambda_{e^+, n})Y_n - (\lambda_{\bar{\nu}_e, p} + \lambda_{e^-, p})Y_p \\ & + \sum_{A(N, Z)} (\lambda_{\nu_e, A(N, Z)} + \lambda_{e^+, A(Z, N)} - \lambda_{\bar{\nu}_e, A(N, Z)} - \lambda_{e^-, A(Z, N)})Y_{A(N, Z)} \end{aligned} \quad (5.1)$$

In general this must be solved together with the other nuclear reactions that occur during nucleosynthesis. To find the approximate form of Y_e from Eq. 5.1, one assumes that the rate of change of conditions is relative slow compared to the weak rates so that $\dot{Y}_e \approx 0$. It assumes also that electron capture can be neglected and that there are no nuclei at all in the composition. For r -process scenarios this sort of approximation is useful when estimating the size of effects that operate before the composition shifts from nucleons to nuclei, such as the effect of weak magnetism [77]. This, however, is not the case for flavor transformation. Fig. 5 shows a comparison between the equilibrium electron fractions to the electron fractions as determined in the full nucleosynthesis calculation for cases both with and without oscillations. The equilibrium calculations of Y_e deviate from the full calculations even early on. By the time the swap occurs, the weak reactions have slowed and the composition has shifted from nucleons to nuclei, and so the equilibrium Y_e no longer provides even an approximate estimate of the nucleosynthetic outcome.

6. Collective oscillations in a full nucleosynthesis network calculation

Our simulations using the full neutrino oscillation calculation results with the nuclear network calculation as described above support the qualitative conclusions from the toy model. As described above, we ran a set of simulations with hydrodynamic trajectories using two density profiles, each with a variety of entropies, $s/k = 100, 200, 300$, and a range of initial timescales, $1 \text{ ms} < \tau < 50 \text{ ms}$. In this section we describe a few cases that illustrate the overall effects of collective oscillations observed in this set of simulations.

We begin by examining the consequences of collective neutrino flavor transformation in our model, and comparing the results of single angle to the results of multiangle calculations. Fig. 6 shows sample final r -process abundance distributions versus mass number A from simulations using the early-time density profile with entropy $s/k = 200$ and timescale $\tau = 15 \text{ ms}$. The simulations have the same hydrodynamic trajectory but varying neutrino physics: one simulation assumes no neutrino oscillations, a second simulation incorporates oscillations calculated in the single-angle approximation, and the third uses a full multiangle calculation

for the oscillations. These are compared to a simulation where neutrino interactions are turned off at $T_9 \sim 9$. Note that the influence of the flavor transformations here is to enhance the influence of neutrino interactions on the r -process and further weaken the third r -process peak. In the single-angle calculation, the third peak is entirely absent.

These results can be understood by examining the early-stage nucleosynthesis depicted in Fig. 7, which shows the evolution of the free neutron abundance and the alpha particle mass fraction through the formation of r -process seeds. In the multiangle calculation, the flavor transformation occurs around $r \sim 100$ km or so, late in the alpha particle formation stage, so here the oscillations tend to intensify an alpha effect that also exists in the case without oscillations. This multiangle case is most similar to the purple line in the toy model shown in Fig. 1, where a swap was introduced at the time when heavy nuclei begin to form. When using the oscillation calculation with the single angle approximation, however, the flavor transformation occurs much earlier, while the initial neutron-to-proton ratio is still being set. This results in a sufficiently large drop in the free neutron abundance to prevent the formation of the third r -process peak. This latter case is similar to the red line in Fig. 1, where a swap was introduced at the beginning of alpha particle formation. In this situation, the inclusion of collective oscillations makes an (erroneously) large impact on the abundance distribution. This single angle approximation is inadequate because it predicts that the oscillation begins too early in the nucleosynthetic process: the composition of the material at the point where the oscillation begins plays a major role in determining the outcome.

We now compare the results discussed above to those with a calculation where the entropy have been altered (the timescale has been correspondingly adjusted to ensure appropriate r -process conditions in the absence of oscillations). Fig. 8 shows sample results from a set of simulations using a higher entropy trajectory. Here we use an early-type density profile with entropy $s/k = 300$ and timescale $\tau = 35$ ms, and show results for simulations with no oscillations and with the full multiangle calculation for the oscillations. Note here the influence of the oscillations is stronger than in Fig. 6; higher entropy pushes the nucleosynthesis farther from the PNS, and so here the flavor transformations occur at a somewhat earlier stage in the nucleosynthesis. Furthermore the timescale is slower, which means that the material experiences a larger neutrino fluence, i.e. more neutrinos and antineutrinos capture on nucleons, and this accentuates the effect of oscillations. Thus, the impact of flavor transformation is dependent on the thermodynamic and hydrodynamic conditions.

We also consider the effect on the final abundance pattern due to the neutrino hierarchy. The top panel of Fig. 8 was produced with an inverted hierarchy, but in the bottom panel a normal hierarchy was used. As long as the μ neutrino luminosity L_{ν_μ} is set to its $q = 3.0$ Keil *et al* value, there is little difference between the normal and inverted hierarchy cases. However the results for the normal hierarchy are quite sensitive to L_{ν_μ} . As can be seen in the figure, a small decrease in the μ neutrino luminosity completely shuts off the collective oscillations in the normal hierarchy. Thus, we find that in some cases, the results will be insensitive to the hierarchy. However, in the more general case, for a given set of electron neutrino and anti-electron neutrino spectra, it is a combination of the hierarchy and the μ

neutrino luminosity that determines the initial starting point of the flavor transformations as well as the course that the oscillation takes.

Finally, we investigate the results for a different density profile, which has lower densities at a given radius than the one we have used thus far. Fig. 9 shows results of simulations using a late-type density profile, here with entropy $s/k = 200$ and initial timescale 18 ms. Nucleosynthesis moves inward, as shown in Fig. 10, and so the flavor transformations occur at a later stage and the influence is similar, but slightly reduced. Still, the size of the effect is similar to that which arises from uncertainties in the nuclear physics inputs, as shown in, for example, Fig. 2 in [78] or Fig. 7 from [79].

Approximate radii for each stage of the nucleosynthesis are listed in Table 1. Taken together with the toy model presented Section 2, one can make a rough guess of the likely impact of collective flavor transformation if one knows the point at which collective oscillation begin (which depends on the neutrino spectra and luminosities). However, we caution that we have found that significant deviations from this rough guess can occur depending on the phase of the oscillation at each point in the evolution of the composition of the material.

7. Conclusion

We establish, using full three neutrino flavor multi-angle calculations, that the flavor transformation can begin in regions sufficiently close to the center of a proto-neutron star that the outcome of element synthesis in hot outflows is appreciably affected. Further, the effect on the final abundance distribution is comparable to that which stems from uncertainties in the nuclear conditions, e.g. [78, 79]. Neutrino collective oscillations act to enhance the role that neutrinos play in r -process nucleosynthesis, and decreases the efficacy of the rapid neutron capture process. We find that the effect of collective flavor transformation can be dramatically overestimated if the “single-angle” approximation is made. An observable effect on the abundance pattern can occur in both the normal and inverted hierarchy. We find that the outcome is dependent not only on the spectra and luminosity of the electron and antielectron neutrinos but also on the μ - and τ -type neutrino spectra.

We stress again that the nucleosynthesis calculations are sensitive to how collective oscillations develop early on, whereas neutrino signal in a terrestrial detector measures the final spectra after the oscillations cease. There are known cases where the final spectra come out qualitatively similar in the single-angle and multiangle calculations, even though at the intermediate stages the spectra are radically different [67]. In this sense, the nucleosynthesis calculations place high demands on the accuracy of the oscillations calculations.

We continue the tradition of studying neutron rich outflows from proto-neutron stars that might occur in supernovae. While self-consistent models which produce a sufficiently neutron rich environment in these conditions have remained elusive, this site remains under consideration as a potential environment due to a variety of astrophysical indicators that favor core-collapse supernovae as the origin of the “main” r -process elements. If and when a self consistent model of a hot outflow is produced, we have shown that these neutrino flavor

transformation effects will need to be included. In the scenarios we have considered, the flavor transformation effects make it more difficult to produce r -process nuclei. However, one must keep in mind that if new, more neutron rich possibilities are discovered, the flavor transformation effects could potentially work in the direction of improving the comparison with abundance data.

Our work improves on previous efforts to estimate the effect of the r -process in two important ways. (1) We use three flavor multi-angle calculations as opposed to “single angle” and/or two flavor calculations. (2) We couple our three flavor multi-angle calculation to a nuclear reaction network so that we include the effects of material composition. These are both essential for making reasonable quantitative estimates of the impact of flavor transformation.

There are a variety of types of elements that are made in the presence of a strong neutrino flux. This type of environment occurs in supernovae near proto-neutron stars, and in compact object mergers and gamma ray bursts from disks around black holes, e.g. [16, 29, 80]. In these strong neutrino fluxes, as we have discussed, neutrinos can be expected to transform collectively. While it may be possible to find some environments with hot outflows where the abundance yields are unaffected by neutrino flavor transformation, this is not clear a priori. The analysis presented here suggests that flavor transformation must be considered in order to predict accurate abundance yields in environments with strong neutrino fluxes.

Acknowledgments

This work was supported in part by DOE contract DE-FG02-02ER41216 (GCM) and DE-FG05-05ER41398 (RS), by the DOE topical collaboration, “Neutrinos and Nucleosynthesis in Hot and Dense Matter” (HD, AF, and GCM), and by LANL LDRD program (HD and AF).

References

- [1] G. M. Fuller, R. W. Mayle, J. R. Wilson and D. N. Schramm, *Astrophys. J.* **322**, 795 (1987)
- [2] D. Notzold and G. Raffelt, *Nucl. Phys. B* **307**, 924 (1988).
- [3] J. T. Pantaleone, *Phys. Rev. D* **46**, 510 (1992).
- [4] J. T. Pantaleone, *Phys. Lett. B* **287**, 128 (1992).
- [5] G. Sigl and G. Raffelt, *Nucl. Phys. B* **406**, 423 (1993).
- [6] B. H. J. McKellar and M. J. Thomson, *Phys. Rev. D* **49**, 2710 (1994).
- [7] Y. Z. Qian, G. M. Fuller, G. J. Mathews, R. Mayle, J. R. Wilson and S. E. Woosley, *Phys. Rev. Lett.* **71**, 1965 (1993).
- [8] J. T. Pantaleone, *Phys. Lett. B* **342**, 250 (1995) [arXiv:astro-ph/9405008].
- [9] Y. Z. Qian and G. M. Fuller, *Phys. Rev. D* **51**, 1479 (1995) [arXiv:astro-ph/9406073].
- [10] G. Sigl, *Phys. Rev. D* **51**, 4035 (1995) [arXiv:astro-ph/9410094].
- [11] S. Pastor and G. Raffelt, *Phys. Rev. Lett.* **89**, 191101 (2002) [arXiv:astro-ph/0207281].

- [12] A. B. Balantekin and H. Yuksel, *New J. Phys.* **7**, 51 (2005) [arXiv:astro-ph/0411159].
- [13] H. Duan, G. M. Fuller, J. Carlson and Y. Z. Qian, *Phys. Rev. D* **74**, 105014 (2006) [arXiv:astro-ph/0606616].
- [14] H. Duan, G. M. Fuller, J. Carlson and Y. Z. Qian, *Phys. Rev. Lett.* **97**, 241101 (2006) [arXiv:astro-ph/0608050].
- [15] S. Chakraborty, S. Choubey, S. Goswami and K. Kar, *JCAP* **1006**, 007 (2010) [arXiv:0911.1218 [hep-ph]].
- [16] R. Surman, G. C. McLaughlin, W. R. Hix, *Astrophys. J.* **643**, 1057-1064 (2006). [astro-ph/0509365].
- [17] B. Metzger, T. A. Thompson, and E. Quataert, *Astrophys. J.* **676** (2008) 1130
- [18] P. S. Barklem, N. Christlieb, T. C. Beers, et. al., *Astron. Astrophys.* **439** (2005) 129
- [19] I. U. Roederer, K.-L. Kratz, A. Frebel, N. Christlieb, B. Pfeiffer, J. Cowan, and C. Sneden, *Astrophys. J.* **698** (2009) 1963
- [20] M. E. Burbidge, G. R. Burbidge, W. A. Fowler and F. Hoyle, *Rev. Mod. Phys.* **29** (1957) 547
- [21] A. G. W. Cameron, Chalk River Rep. **CRL-41** (1957)
- [22] M. Arnould, S. Goriely, and K. Takahashi, *Phys. Rept.* **450** (2007) 97
- [23] C. Sneden, A. McWilliam, G. W. Preston, J. Cowan, D. L. Burris, and B. J. Armosky, *Astrophys. J.* **467** (1996) 819
- [24] S. G. Ryan, J. E. Norris, and T. C. Beers, *Astrophys. J.* **471** (1996) 254
- [25] Y. Ishimaru and S. Wanaajo, *Astrophys. J.* **511** (1999) L33
- [26] J. W. Truran, J. J. Cowan, A. Pilachowski, and C. Sneden, *Pub. Astron. Soc. Pac.* **114** (2002) 1293
- [27] B. S. Meyer, *Astrophys. J.* **343** (1989) 254
- [28] C. Frieburghaus, S. Rosswog, and F.-K. Thielemann, *Astrophys. J.* **525** (1999) L121
- [29] R. Surman, G. C. McLaughlin, M. Ruffert *et al.*, *Astrophys. J.* **679**, L117 (2008). [arXiv:0803.1785 [astro-ph]].
- [30] D. Argast, M. Samland, F.-K. Thielemann, and Y.-Z. Qian, *Astron. Astrophys.* **416** (2004) 997
- [31] S. Wanaajo and I. Ishimaru, *Nucl. Phys. A* **777** (2006) 676
- [32] B. S. Meyer, G. J. Mathews, W. M. Howard, S. E. Woosley, and R. D. Hoffman, *Astrophys. J.* **399** (1992) 656
- [33] S. E. Woosley, J. R. Wilson, G. J. Mathews, R. D. Hoffman, and B. S. Meyer *Astrophys. J.* **433** (1994) 229
- [34] K. Takahashi, J. Wittl, and H.-Th. Janka, *Astron. Astrophys.* **286** (1994) 857
- [35] G. M. Fuller and B. S. Meyer, *Astrophys. J.* **453** (1995) 792
- [36] G. C. McLaughlin, G. M. Fuller, J. R. Wilson, *Astrophys. J.* **472**, 440 (1996). [astro-ph/9701114].

- [37] B. S. Meyer, G. C. McLaughlin, G. M. Fuller, *Phys. Rev.* **C58**, 3696-3710 (1998). [astro-ph/9809242].
- [38] Y.-Z. Qian and S. E. Woosley, *Astrophys. J.* **471** (1996) 331
- [39] R. D. Hoffman, S. E. Woosley, and Y.-Z. Qian, *Astrophys. J.* **482** (1997) 951
- [40] T. A. Thompson, A. Burrows, and B. S. Meyer, *Astrophys. J.* **562** (2001) 887
- [41] M. Terasawa, K. Sumiyoshi, S. Yamada, et. al., *Astrophys. J.* **578** (2002) L137
- [42] M. Liebendorfer, M. Rampp, H.-Th. Janka, and A. Mezzacappa, *Astrophys. J.* **620** (2005) 840
- [43] S. Wanajo, *Astrophys. J.* **650** (2006) L79
- [44] C. Fryer, *Astrophys. J.* **699** (2009) 409
- [45] T. Fischer, S. C. Whitehouse, A. Mezzacappa *et al.*, *Astron. Astrophys.* **517**, A80 (2010). [arXiv:0908.1871 [astro-ph.HE]].
- [46] L. Huedepohl, B. Mueller, H.-Th. Janka, A. Marek, and G. G. Raffelt, astro-ph/0912.0260
- [47] J. Gava, J. Kneller, C. Volpe, and G. C. McLaughlin, *Phys. Rev. Lett.* **103** (2009) 071101
- [48] A. Arcones, H.-Th. Janka, and L. Scheck, *Astron. Astrophys.* **467** (2007) 1227
- [49] K. Farouqi, K.-L. Kratz, L. I. Mashonkina, B. Pfeiffer, J. J. Cowan, F.-K. Thielemann, and J. W. Truran, *Astrophys. J.* **694** (2009) L49
- [50] G. Martinez-Pinedo, D. Mocerj, N. T. Zinner, A. Kelic, K. Langanke, I. Panov, B. Pfeiffer, T. Raucher, K.-H. Schmidt, and F.-K. Thielemann, *Prog. Part. Nucl. Phys.* **59** (2007) 199
- [51] J. Beun, G. C. McLaughlin, R. Surman *et al.*, *Phys. Rev.* **C77**, 035804 (2008). [arXiv:0707.4498 [astro-ph]].
- [52] G. C. McLaughlin, J. M. Fetter, A. B. Balantekin *et al.*, *Phys. Rev.* **C59**, 2873-2887 (1999). [astro-ph/9902106].
- [53] J. Fetter, G. C. McLaughlin, A. B. Balantekin *et al.*, *Astropart. Phys.* **18**, 433-448 (2003). [hep-ph/0205029].
- [54] D. O. Caldwell, G. M. Fuller, and Y.-Z. Qian, *Phys. Rev.* **D 61** (2000) 123005
- [55] J. Beun, G. C. McLaughlin, R. Surman *et al.*, *Phys. Rev.* **D73**, 093007 (2006). [hep-ph/0602012].
- [56] B. S. Meyer, *Phys. Rev. Lett.* **89**, 231101 (2002).
- [57] M. Keil, G. G. Raffelt, and H.-Th. Janka, *Astrophys. J.* **590** (2003) 971
- [58] L. Wolfenstein, *Phys. Rev. D* **17**, 2369 (1978).
- [59] S. P. Mikheev and A. Y. Smirnov, *Sov. J. Nucl. Phys.* **42**, 913 (1985) [*Yad. Fiz.* **42**, 1441 (1985)].
- [60] S. P. Mikheev and A. Y. Smirnov, *Sov. Phys. JETP* **64**, 4 (1986) [*Zh. Eksp. Teor. Fiz.* **91**, 7 (1986)] [arXiv:0706.0454 [hep-ph]].
- [61] A. Friedland, *Phys. Rev. D* **64**, 013008 (2001) [arXiv:hep-ph/0010231].

- [62] H. Duan and J. P. Kneller, *J. Phys. G* **36**, 113201 (2009) [arXiv:0904.0974 [astro-ph.HE]].
- [63] H. Duan, G. M. Fuller and Y. Z. Qian, arXiv:1001.2799 [hep-ph].
- [64] A. Friedland and C. Lunardini, *JHEP* **0310**, 043 (2003) [arXiv:hep-ph/0307140].
- [65] H. Duan, G. M. Fuller and Y. Z. Qian, *Phys. Rev. D* **74**, 123004 (2006) [arXiv:astro-ph/0511275].
- [66] A. Esteban-Pretel, A. Mirizzi, S. Pastor, R. Tomas, G. G. Raffelt, P. D. Serpico and G. Sigl, *Phys. Rev. D* **78**, 085012 (2008) [arXiv:0807.0659 [astro-ph]].
- [67] H. Duan and A. Friedland, arXiv:1006.2359 [hep-ph].
- [68] A. Friedland, *Phys. Rev. Lett.* **104**, 191102 (2010) [arXiv:1001.0996 [hep-ph]].
- [69] W. R. Hix and F.-K. Thielemann, *J. Comp. App. Math.* **109** (1999) 321
- [70] R. Surman and J. Engel, *Phys. Rev. C* **64** (2001) 035801
- [71] R. C. Duncan, S. L. Shapiro and I Wasserman, *Astrophys. J.*, **309**, 141 (1986)
- [72] Y. Z. Qian, S. E. Woosley, *Astrophys. J.* **471**, 331-351 (1996). [astro-ph/9611094].
- [73] T. A. Thompson, A. Burrows, B. S. Meyer, *Astrophys. J.* **562**, 887 (2001). [astro-ph/0105004].
- [74] C. Y. Cardall, G. M. Fuller, *Astrophys. J.* **486**, L111 (1997). [astro-ph/9701178].
- [75] M. Terasawa, T. Kajino, K. Langanke *et al.*, *Astrophys. J.* **608** 470 (2004).
- [76] I. V. Panov and H.-Th. Janka, *Astron. Astrophys.* **494** (2009) 829
- [77] C. J. Horowitz, *Phys. Rev. D* **65**, 043001 (2002). [astro-ph/0109209]
- [78] R. Surman, J. Beun, G. C. McLaughlin and W. R. Hix, *Phys. Rev. C* **79**, 045809 (2009) [arXiv:0806.3753 [nucl-th]].
- [79] A. Arcones, G. Martinez-Pinedo, [arXiv:1008.3890 [astro-ph.SR]].
- [80] Metzger, B. D., Thompson, T. A., & Quataert, E. *Astrophys. J.* **659**, 561 (2007)

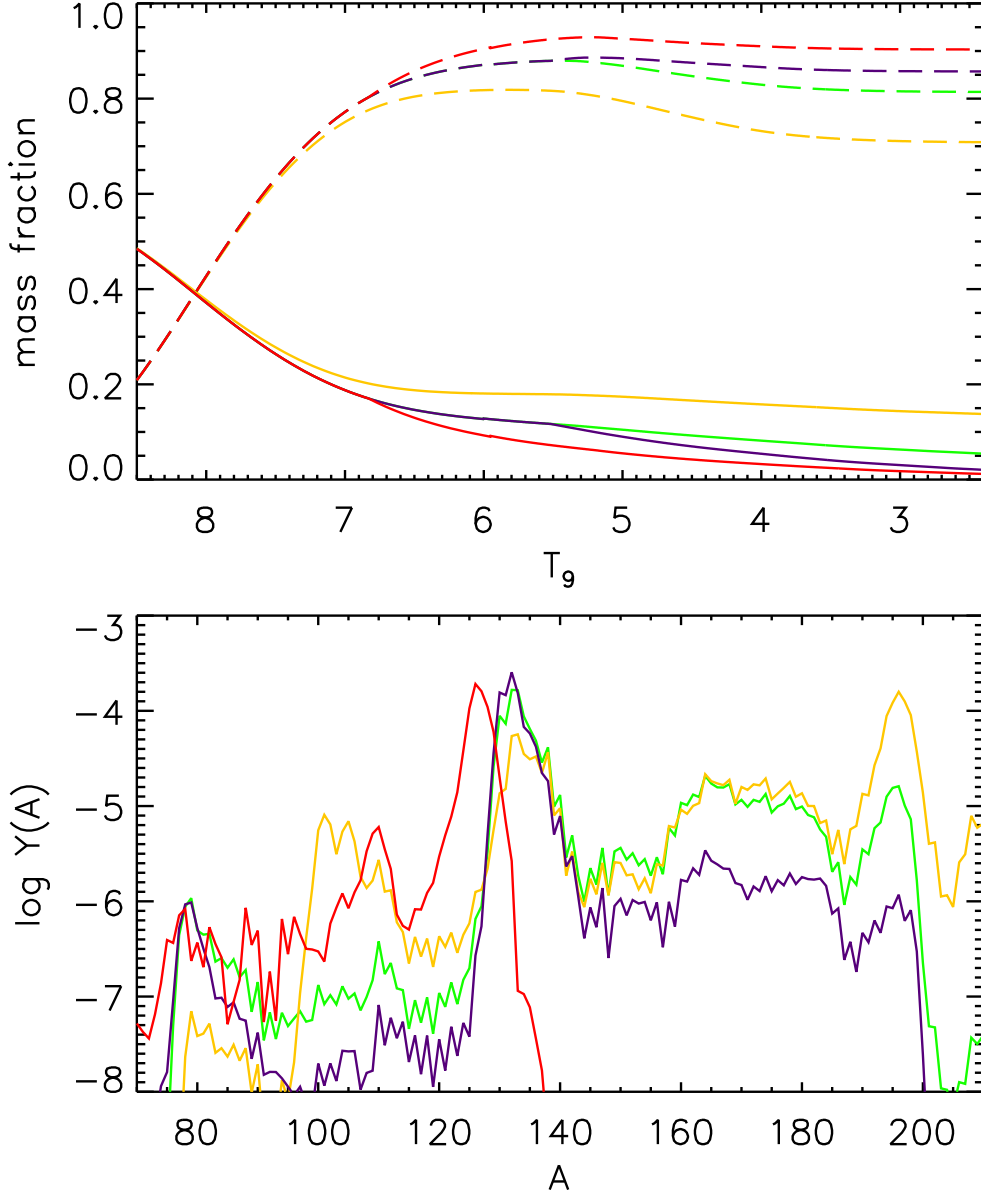


Figure 1: The upper panel shows the mass fractions of neutrons (solid lines) and alpha particles (dashed lines) for sample simulations with no neutrino oscillations (green), a test neutrino swap that occurs at the point of alpha particle assembly into heavier nuclei (purple), a test neutrino swap that occurs during assembly of nucleons into alphas (red), and neutrino interactions turned off for $T_9 < 9$ K (yellow). The bottom panel shows the final r -process abundances for each of the simulations. All simulations use the same hydrodynamic trajectory, with a timescale of 20 ms and an entropy of $s/k = 200$, and the neutrino fluxes are the $q = 3.0$ case from [57].

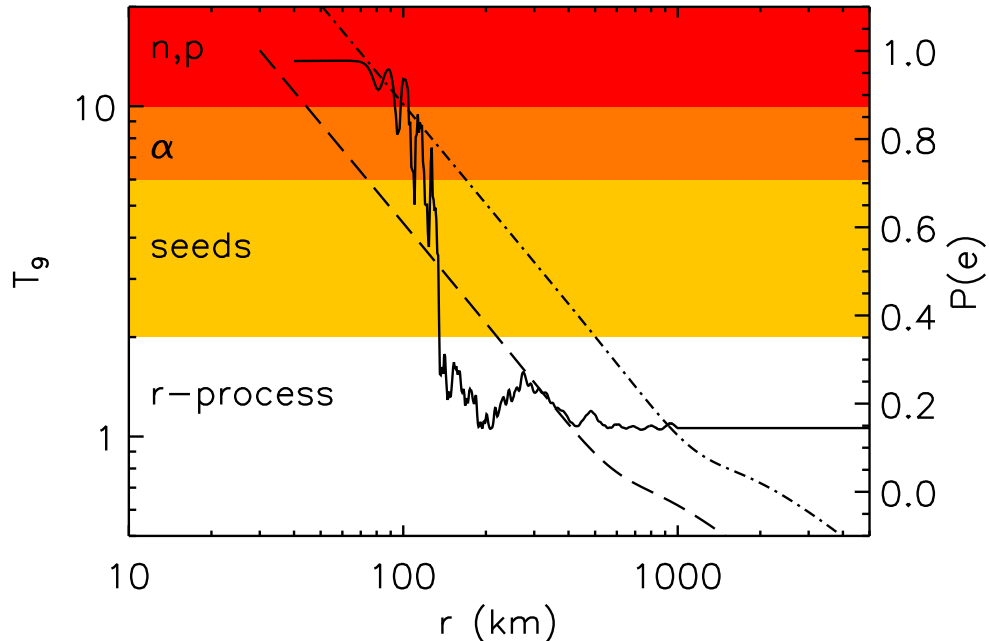


Figure 2: Shows temperature T_9 as a function of radius in km (dashed line) for two sample thermodynamic trajectories, one with lower density and $s/k = 300$ (dot-dashed line) and the other with higher density and $s/k = 200$ (dashed line); the horizontal bands show the approximate temperature ranges for each stage of the nucleosynthesis as labeled. The solid line shows a sample electron neutrino survival probability $P(e)$ for 20 MeV neutrinos, as calculated assuming an inverted hierarchy. For the trajectory with the early-type density profile, the flavor transformations occur during alpha particle formation, while for the trajectory with the late-type density profile the flavor transformations occur later, during the r -process seed assembly.

s/k	density profile	R_α (km)	R_{seed} (km)	$R_{r\text{-process}}$ (km)
100	early-type	80	120	350
200	early-type	100	170	440
300	early-type	120	200	500
100	late-type	40	60	175
200	late-type	50	85	220
300	late-type	60	100	250

Table 1: Shows the approximate radii in km at which various stages of the nucleosynthesis begin for a range of thermodynamic trajectories. We define R_α (R_{seed}) as the radius at which the mass fraction of alpha particles (seed nuclei) is 10% of its maximum value, and $R_{r\text{-process}}$ is the radius at which $T_9 \sim 2$.

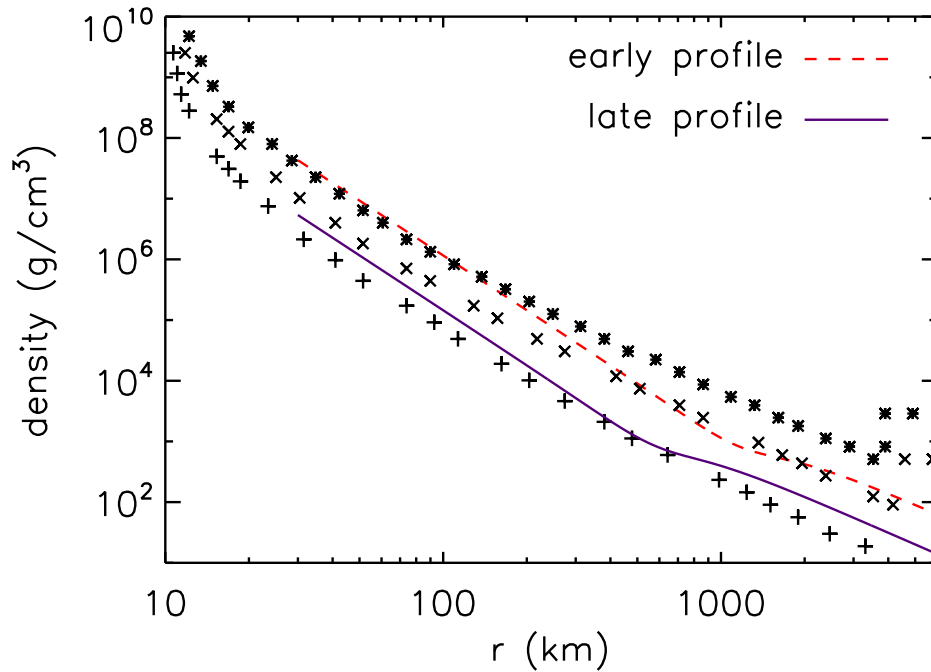


Figure 3: Shows two sample density profiles—an early-type profile (dashed line) and a late-type profile (solid line)—used in this work. To show the similarities between our parameterized profiles and recent hydrodynamical calculations, we also include profiles extracted from Arcones *et al* [48], corresponding to $t = 2$ s (asterisks), $t = 4$ s (x's), and $t = 10$ s (crosses) after core bounce.

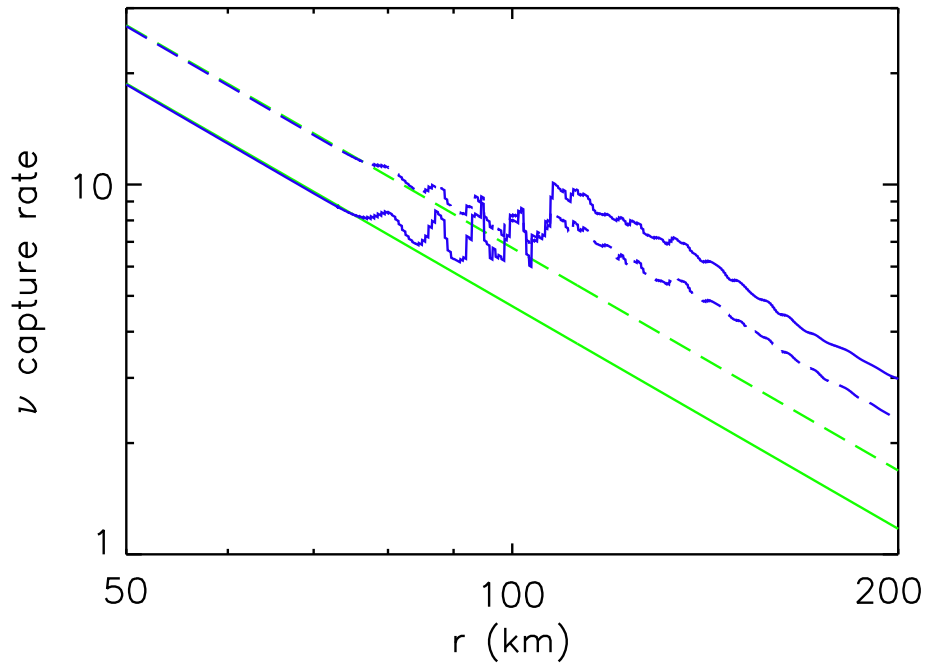


Figure 4: Shows electron neutrino (solid line) and electron antineutrino (dashed line) capture rates per nucleon as a function of radius in km for the neutrino fluxes with no oscillations (green) and with the full multiangle oscillation calculation (blue), assuming an inverted hierarchy for the neutrino masses. The neutrino fluxes are the $q = 3.0$ case from [57], with neutrino temperatures $T_{\nu_e} = 2.6$, $T_{\bar{\nu}_e} = 4.0$, and $T_{\nu_\mu} = 5.0$, degeneracy parameters $\eta_{\nu_e} = 3.0$, $\eta_{\bar{\nu}_e} = 2.8$, and $\eta_{\nu_\mu} = 1.8$, and luminosities $L_{\nu_e} = 6.6 \times 10^{51}$ ergs s^{-1} , $L_{\bar{\nu}_e} = 8.8 \times 10^{51}$ ergs s^{-1} , and $L_{\nu_\mu} = 12.7 \times 10^{51}$ ergs s^{-1} .

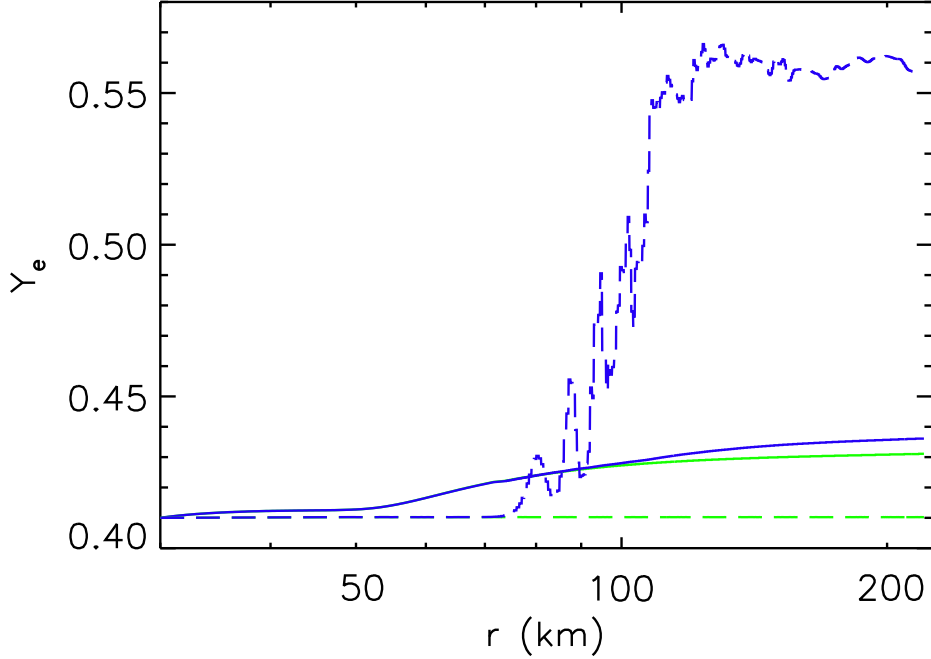


Figure 5: Shows the electron fraction as a function of radius in km for the full nucleosynthesis calculation described in Sec. 4 for an example hydrodynamic trajectory and varying treatments of the neutrino physics—no oscillations (green line) and oscillations in the full multiangle calculation (blue line). These are compared to the electron fractions calculated using the approximate formula $Y_e = 1 / \left(1 + \frac{\lambda_{\nu_e}}{\lambda_{\nu_e}} \right)$ for cases with no oscillations (dashed green line) and with the full multiangle oscillation calculation (dashed blue line). All oscillation calculations here assume an inverted hierarchy for the neutrino masses, and the neutrino rates used here are those of Fig. 4.

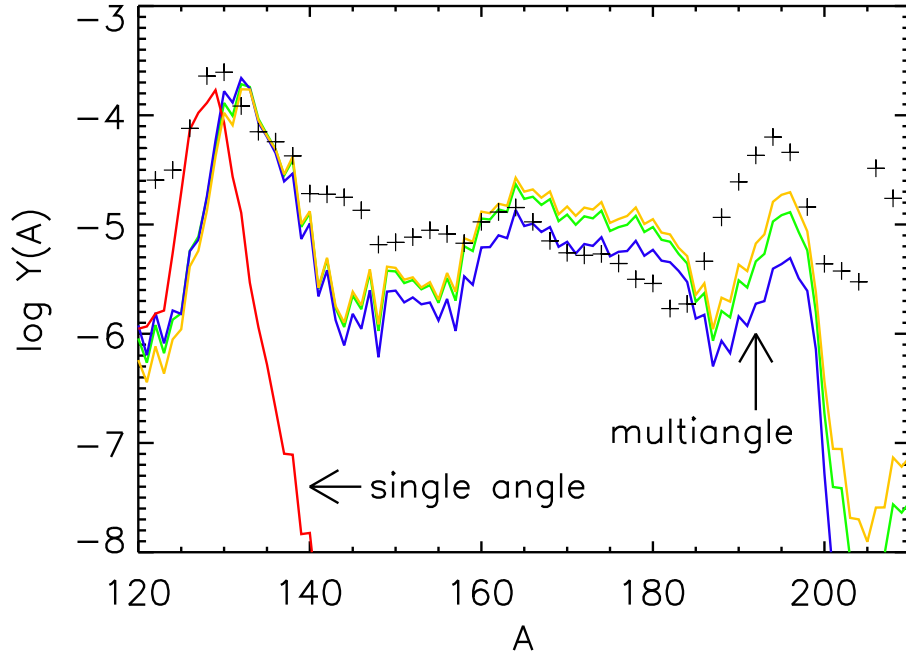


Figure 6: Shows final abundances Y versus mass number A for simulations with no neutrino oscillations (green) and single-angle (red) and full multiangle (blue) oscillation calculations, both assuming an inverted hierarchy. Scaled solar abundances (crosses) and the results of a simulation with neutrino interactions turned off at $T_9 \sim 9$ (yellow) are shown for comparison. All four simulations use the early-type density profile with entropy $s/k = 200$ and initial timescale $\tau = 15$ ms.

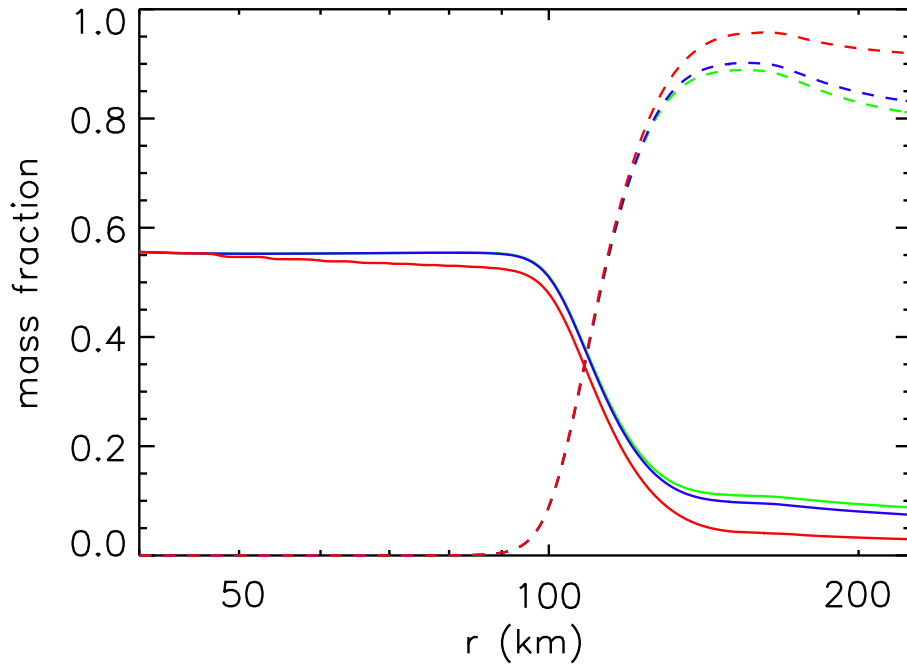


Figure 7: Shows mass fractions of neutrons (solid lines) and alpha particles (dashed lines) as a function of radius r in km for the three simulations from Fig. 6. In the single-angle calculation, the flavor transformations occur early and influence the initial free neutron abundance, while in the multiangle calculation the transformations occur as the alphas are assembling into seeds.

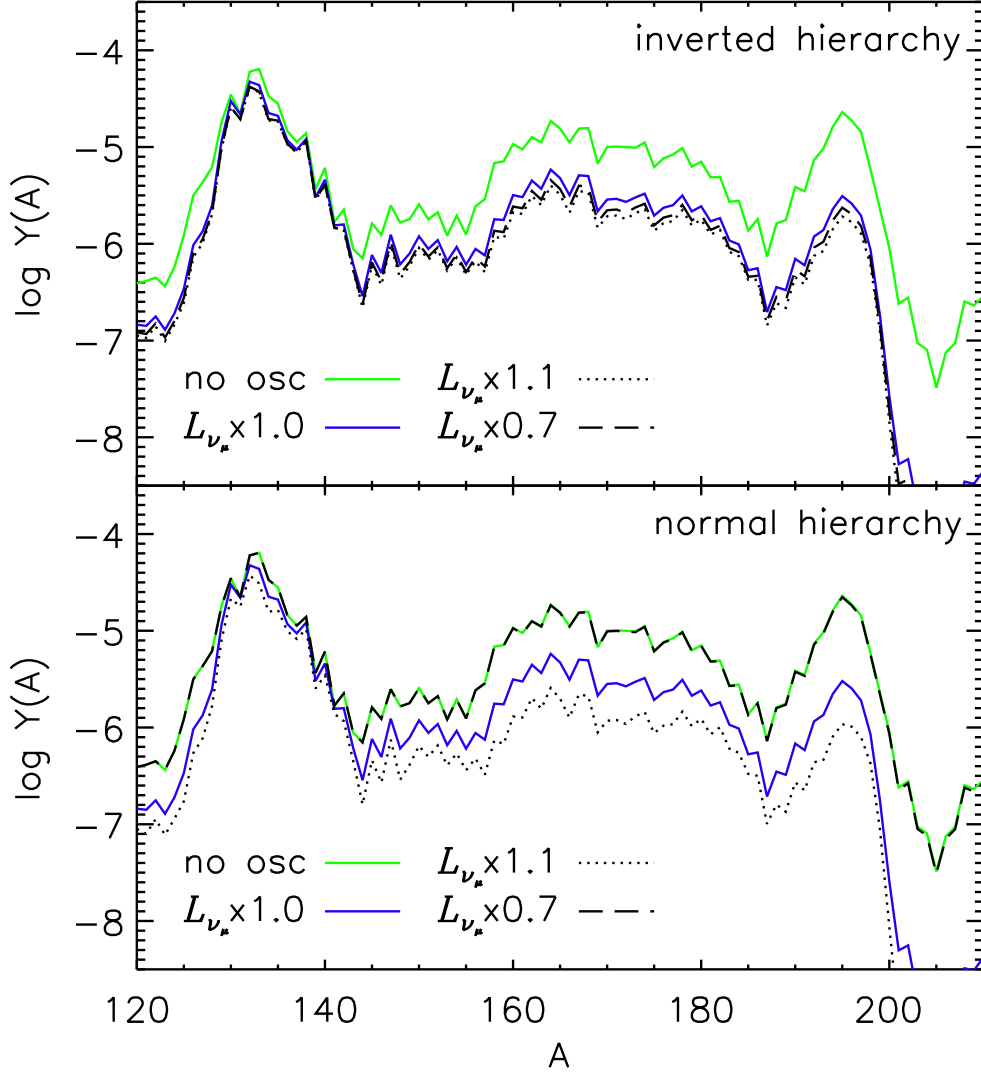


Figure 8: Shows final abundances Y versus mass number A for simulations with no neutrino oscillations (green) and full multiangle oscillation calculations (blue) assuming a normal hierarchy (bottom panel) and inverted hierarchy (top panel). The results from simulations where the μ neutrino luminosity is multiplied by either a factor of 1.1 (dotted line) or 0.7 (dashed line) are also shown for each case. All simulations use the early-type density profile with entropy $s/k = 300$ and initial timescale $\tau = 35$ ms.

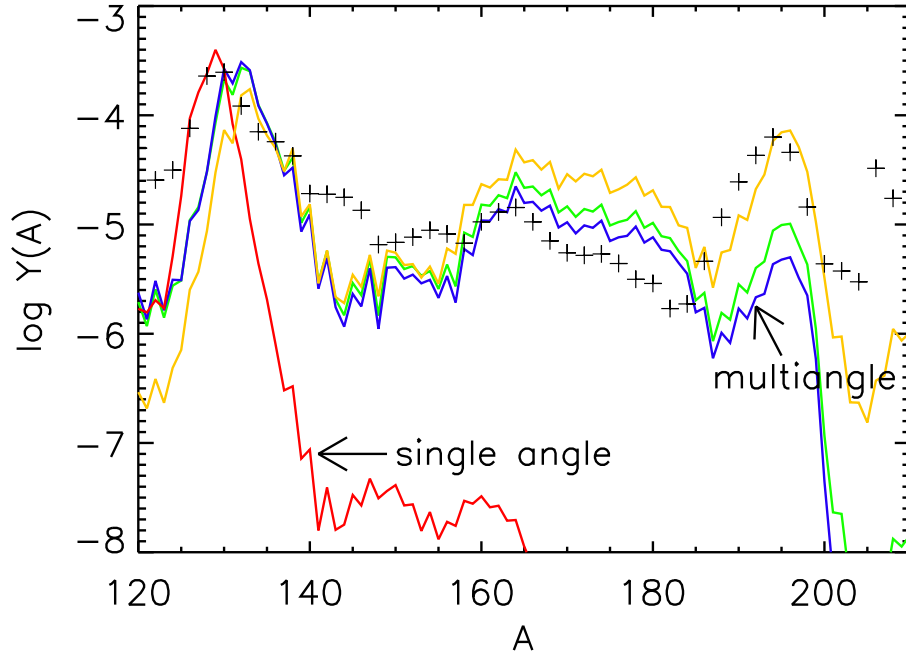


Figure 9: Shows final abundances Y versus mass number A for simulations with no neutrino oscillations (green) and single-angle (red) and full multiangle (blue) oscillation calculations, both assuming an inverted hierarchy. Scaled solar abundances (crosses) and the results of a simulation with neutrino interactions turned off at $T_9 \sim 9$ (yellow) are shown for comparison. All four simulations use the late-type density profile with entropy $s/k = 200$ and initial timescale $\tau = 18$ ms.

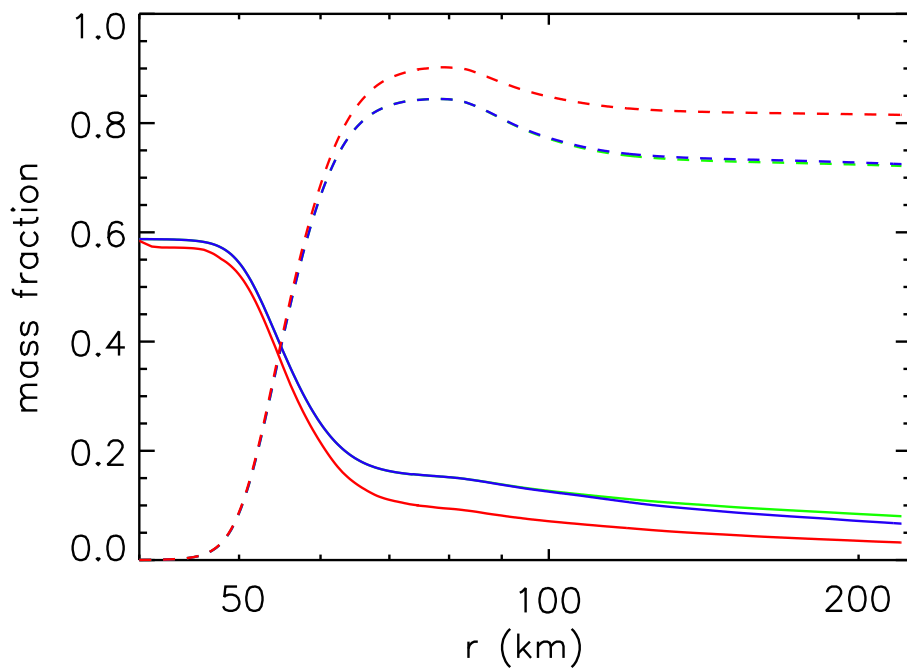


Figure 10: Shows mass fractions of neutrons (solid lines) and alpha particles (dashed lines) as a function of radius r in km for the three simulations from Fig. 9. The flavor transformations occur at a significantly later stage of the nucleosynthesis than in the simulations shown in Fig. 7.